Clays and Clay Minerals, Vol. 48, No. 2, 196–203, 2000.

THE DEPENDENCE OF LOCALIZED CRYSTALLIZATION OF HALLOYSITE AND KAOLINITE ON PRIMARY MINERALS IN THE WEATHERING PROFILE OF GRANITE

GI YOUNG JEONG

Department of Earth and Environmental Sciences, Andong National University, Andong 760-749, Korea

Abstract—The formation of kaolin-group minerals in the weathering profile of granite, under the humid, temperate climate as found in Korea, was studied by X-ray diffraction (XRD), scanning electron microscopy (SEM), and electron microprobe analysis (EMA). The granite was gradually weathered to saprolite. K-rich feldspar was not weathered in the profile, but plagioclase partially weathered to halloysite septa (*i.e.*, wall-like masses). At the bottom of the profile, biotite had weathered to regularly interstratified biotite-vermiculite (B-V), and subsequently to kaolinite, with a considerable increase in grain volume. In the upper part of the profile, loose aggregates of transported clays, including halloysite and kaolinite, coated the preformed halloysite septa in the weathered plagioclase. Halloysite had precipitated as a metastable phase in the microfissures of partially weathered plagioclase. Kaolinite had precipitated heavily in the weathered biotite, where surfaces supply abundant templates facilitating the nucleation of kaolinite. The localized crystallization of halloysite and kaolinite, depending on the distribution of primary minerals, strongly influenced the kaolin mineralogy of the granite weathering profile.

Key Words—Biotite, Granite, Halloysite, Kaolinite, Weathering.

INTRODUCTION

Under a temperate and humid climatic regime, primary aluminosilicate minerals are usually weathered to kaolin-group minerals, either directly, or through various intermediates of 2:1 phyllosilicates, such as smectites, vermiculites, and interstratified clay minerals. Halloysite and kaolinite are the most common kaolin minerals in these weathering environments (Keller, 1977; Gilkes *et al.*, 1980; Keller *et al.*, 1980; Banfield and Eggleton, 1990; Schroeder *et al.*, 1997). The common coexistence of these two minerals in the weathering profile attracts much interest because of their chemical and structural similarity. Their relative abundances were known to change within one weathering profile, or from one to another profile (Parham, 1969). Transformations between the two minerals after their early formation may change their relative abundances, as suggested by thermodynamic and kinetic simulation (Steefel and Van Cappellen, 1990), by microscopic observations (Churchman and Gilkes, 1989; Robertson and Eggleton, 1991; Singh and Gilkes, 1992; Singh and Mackinnon, 1996; Jeong, 1998a), and by structural modeling (Singh, 1996). The abundances of kaolin minerals in the relatively young weathering profile appear to be largely controlled by the different formation processes because transformations require time. In the study of the weathering profiles of anorthosite, plagioclase was commonly weathered to halloysite (Jeong and Kim, 1993), and primary phyllosilicates were commonly weathered to kaolinite (Jeong, 1998b). These results suggest the importance of the primary mineral structure on kaolin mineralogy in weathering profiles. The influence of the primary mineral structure should be identified in the weathering profiles of more widely distributed rocks, such as granite. This paper reports the localized crystallization of halloysite and kaolinite, depending on the primary minerals in the weathering profile of granite under a humid, temperate climate regime in Korea.

STUDY AREA

An ellipsoidal granite batholith is exposed to the north of Taegu City, Korea (Figure 1). The K-Ar radiogenic age (Lee, 1987) of the biotite is 82 million years ago. The granite consists of quartz (29.5 wt. %), K-rich feldspar (30.8 wt. %), plagioclase (31.1 wt. %), biotite (4.8 wt. %), amphibole (2.8 wt. %), opaque minerals (1.0 wt. %), and minor zircon and apatite. Plagioclase (An_{12}–An_{31}) occurs as subhedral phenocrysts with compositional zoning. Mean annual temperature and precipitation are 13.7°C and 889 mm, respectively. Palgong Mount (1193 m) is located at the center of the granite terrain. The studied weathering profile is exposed at a roadcut in the northern flank of the Palgong Mount. The elevation of the site is 480 m and the slope is 11°. The profile depth is ~6 m.

MATERIALS AND METHODS

Five samples were collected from the weathering profile at depths of 0.1, 1, 3, 5, and 6 m, and stored in polyethylene bottles to preserve the natural moisture. Bulk chemical compositions were analyzed using a Philips PW1480 X-ray fluorescence spectrometer at the Korea Basic Science Institute in Seoul. Weathered plagioclase and biotite were separated by hand under a stereomicroscope, and ground in an agate mortar. X-ray diffraction (XRD) analyses of samples were per-

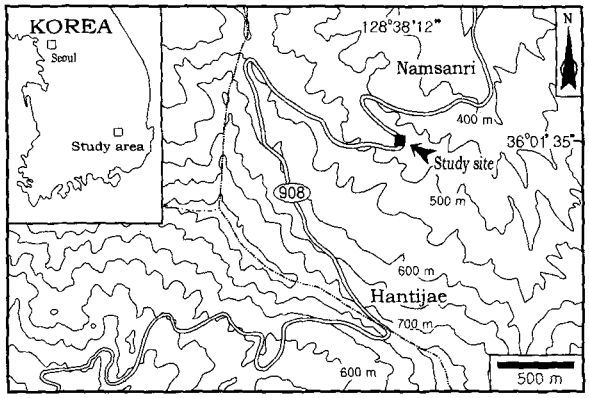

Figure 1. Location map of the weathering profile of granite. The entire area consists of Cretaceous granite.

formed, before drying, using a Siemens D-5005 X-ray diffractometer equipped with a Cu X-ray tube operating at 40 kV, 45 mA, and using 6-mm variable slits, and a 0.2° receiving slit. In addition, weathered biotite was saturated with Mg and subsequently treated with ethylene glycol. Samples were also examined after heating at 350 and 550°C. Samples were impregnated with epoxy resin under vacuum, and polished thin sections were made. Untreated samples and polished thin sections were examined in a Hitachi S2500 scanning electron microscope (SEM) equipped with a Kevex energy dispersive X-ray analyzer. Samples were examined by using secondary electrons. The contrast of the secondary-electron images of the flat surface of the thin sections was optimized by using a large condenser-lens aperture and reducing the condenser-lens current. Chemical compositions of the weathering products of plagioclase and biotite were determined with a Cameca SX51 electron microprobe analyzer (EMA) at the Korea Basic Science Institute in Taejon under the following conditions: 15 kV, 10 nA, 10-s counting time, and 5-μm beam diameter.

RESULTS

General characteristics of weathering profile

The weathering profile of granite showed many characteristics of saprolite. The weathered granite showed well-preserved arrangements and shapes of the primary minerals relative to the original, without notable disturbance throughout the profile. The original structure of the granite was lost only in the uppermost part (less than ~10 cm) owing to pedoturbation. Active erosion on the slopes prevented thick residual accumulation of soil materials and full development of soil horizons. Table 1 shows chemical variations in the weathering profile of the granite. Decreases in Na_2O and CaO content and an increase in loss-on-ignition upwards in the profile is explained by dissolution of plagioclase and formation of clay minerals, respectively. Nearly constant K_2O content suggests the non-weatherability of K-rich feldspar which was confirmed by microscopic observation of thin sections.

Plagioclase weathering

XRD patterns of the weathered plagioclase are shown in Figure 2. Slightly weathered plagioclase in the lowermost part of the profile at a depth of 6 m does not show a basal peak typical of clay minerals, but a weak 4.4-Å peak occurs. Weathered plagioclases of the middle part of the profile at depths of 3 and 5 m show 10-Å peaks and asymmetrical diffraction bands at 4.44 Å, both indicating the formation of clay minerals. Weathered plagioclases in the upper part of the profile at depths of 0.1 and 1 m show more intense 10-Å peaks and weak 7.20–7.24-Å peaks. On heating at 60°C, 10-Å peaks are replaced by 7.35-Å peaks. Subsequent formamide intercalation (Churchman *et al.,* 1984) for the dehydrated samples reexpands the phases producing 7.35-Å peaks to phases having 10.2-Å peaks. Resulting patterns have 7.23–7.26-Å peaks whose intensities are similar to those of untreated samples. Therefore, the phases producing 10-Å and 7.20–7.24-Å peaks are ascribed to hydrated halloysite and kaolinite, respectively. In natural weathering environments of deep saprolite, halloysite usually occurs in a hydrated form (Jeong, 1992). Integrated peak areas were measured for the 10-Å and 7.20–7.24-Å peaks in Figure 2, and converted to the relative-weight proportions of halloysite and kaolinite, respectively, by using the relative-intensity data measured against corundum as described by Jeong (1992). The halloysite to kaolinite ratios in samples at depths of 0.1 and 1 m were 5.7 and 3.3, respectively.

Table 1. Bulk oxide chemistry of the samples studied in the weathering profile of granite.

Depth of sample	Bulk chemistry (wt. %)											
	SiO_2	Al_2O_3	Fe_2O_3	MgO	TiO_2	MnO	CaO	K_2O	Na_2O	P_2O_5	L.I.[1]	Total
0.1 m	66.73	18.58	4.25	0.70	0.51	0.05	0.36	3.76	0.68	0.02	7.15	99.78
1 m	66.15	17.60	3.92	0.68	0.49	0.05	0.42	3.96	0.86	0.02	6.48	99.62
3 m	65.63	17.17	3.96	1.03	0.51	0.07	1.10	3.83	1.66	0.02	4.80	99.78
5 m	67.13	16.30	3.57	1.04	0.45	0.06	1.29	3.82	2.06	0.02	3.85	99.57
6 m	69.97	14.70	3.14	1.00	0.40	0.04	1.91	3.85	3.16	0.02	1.52	99.71

[1] Loss on ignition.

https://doi.org/10.1346/CCMN.2000.0480205 Published online by Cambridge University Press

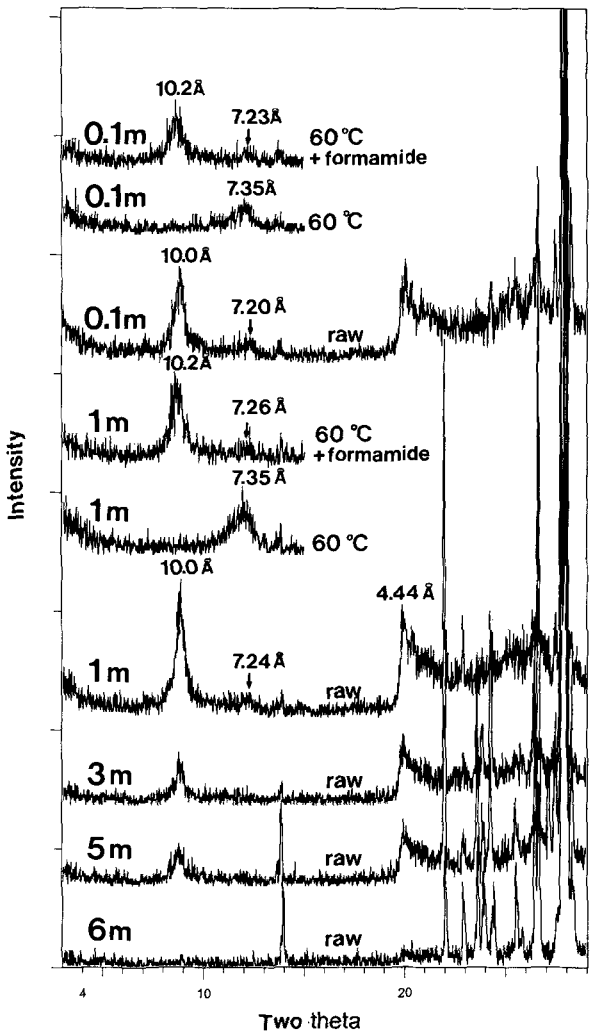

Figure 2. XRD patterns of the untreated and treated specimens of weathered plagioclases at various depths.

The SEM photograph of a thin section of the sample at a depth of 3 m shows compact clay septa (*i.e.*, wall-like masses) filling the widened microfissures of partially dissolved plagioclase (Figure 3a). The septa have the chemical composition of kaolin (Table 2). The SEM photograph of the corresponding untreated sample shows compact aggregates of complexly interlacing halloysite tubes in microfissures, and skeletal plagioclase grains with clean surfaces (Figure 3b and 3c). The microtextures of compact halloysite septa indicate an *in situ* growth in the microfissures of the weathered plagioclase, as reported in detail by Jeong and Kim (1993).

The SEM photograph of a thin section of the (uppermost) sample at a depth of 0.1 m shows compact halloysite septa (Figure 4a). The skeletal plagioclase grains preserve the crystallographic orientation of the original large phenocryst. In contrast to extensive dis-

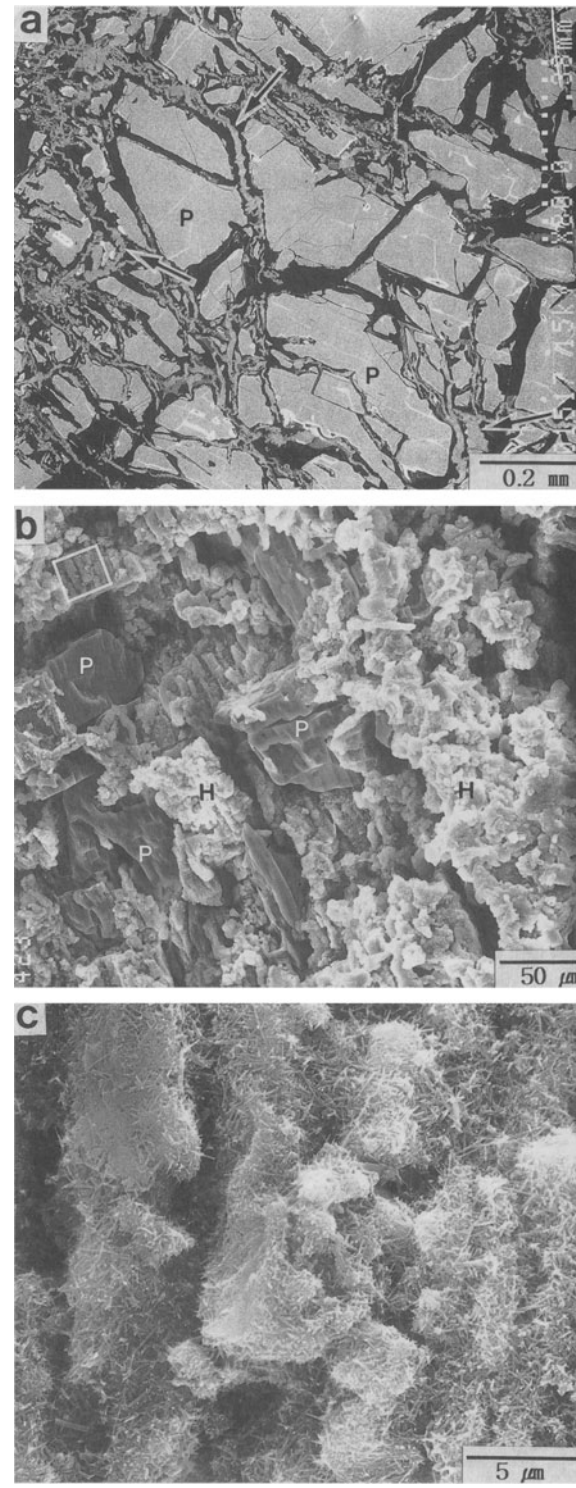

Figure 3. SEM photographs of the weathered plagioclase at a depth of 3 m. a) Thin section: halloysite septa (arrows), skeletal plagioclase (P) grains, and voids (black). b) Untreated sample: halloysite aggregates and skeletal plagioclase grains with a clean surface. c) Enlarged image of the box in (b) showing the compact aggregates of complexly interlacing halloysite tubes.

https://doi.org/10.1346/CCMN.2000.0480205 Published online by Cambridge University Press

Table 2. Electron-microprobe data (wt. % oxide) of clays in the microfissures of plagioclase.

	Compact halloysite septa			Loose kaolin aggregate	
Oxide	5 m	3 m	0.1 m	1 m	0.1 m
SiO_2	46.71	44.00	48.12	30.34	32.52
Al_2O_3	33.37	32.85	34.91	24.64	25.74
Fe_2O_3	1.85	1.18	1.09	1.92	4.83
MgO	0.98	1.17	0.78	0.25	0.60
TiO_2	0.00	0.00	0.00	0.22	0.47
MnO	0.00	0.07	0.00	0.00	0.01
CaO	0.26	0.20	0.04	0.07	0.05
K_2O	0.08	0.10	0.08	0.14	0.59
Na_2O	0.04	0.06	0.04	0.03	0.10
Total	83.29	79.63	85.07	57.61	64.90

solution of plagioclase, K-rich feldspar and quartz do not show notable dissolution textures. The compact halloysite septa (light gray in the SEM image) are coated with loose accumulations of clay particles (dark gray) (Figure 4b), which are brown under the polarizing microscope. These particles are chemically similar to kaolin (Table 2). The Fe, Ti, and K contents of the loose accumulations are very low, but higher than those of the compact halloysite septa. The low totals of the data from EMA indicate abundant micropores. The SEM photograph of the corresponding untreated sample shows that the accumulations are oriented aggregates of flat-lying tubes and plates, indicating a mixture of halloysite and kaolinite (Figure 4c). The kaolin particles in the loose aggregates appear to have moved into the weathering plagioclase from an external source.

Biotite weathering

The XRD patterns of the oriented and untreated clay-aggregate samples of weathered biotite show strong superlattice reflections of regularly interstratified biotite-vermiculite (B-V) and the 7.24–7.30-Å peaks of kaolin minerals (Figure 5). The $d(00l)$ values of the B-V do not show any notable change after saturation by Mg and ethylene glycol. After heating to 550°C, the XRD pattern indicated that the B-V phase collapsed to 9.9 Å (Figure 6). Biotite proportion of the B-V as estimated from the $d(002)$ (Reynolds, 1981) was ~60%. The peak intensities from the kaolin minerals did not change after formamide intercalation, but the peaks increased in intensity slightly on heating to 350°C, and they completely disappeared at 550°C (Figure 6). XRD data collectively suggest that the 7.24–7.30-Å peaks are produced by kaolinite, whose content in the profile gradually increases upwards.

The SEM photograph of a thin section of the sample at a depth of 6 m shows weathered biotite with an original grain shape (Figure 7a), but EMA revealed that the K content has decreased to about half that of fresh biotite, implying the rapid formation of B-V (Table 3). In the highly weathered biotite at a depth of

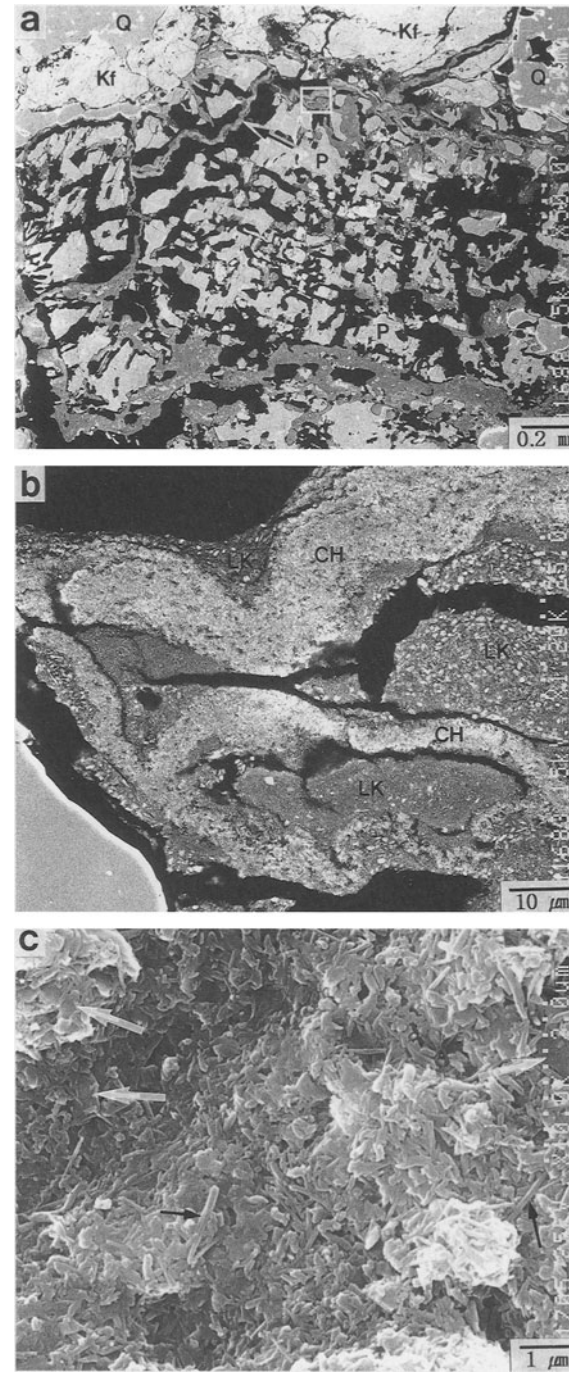

Figure 4. SEM photographs of a weathered plagioclase phenocryst at a depth of 0.1 m. a) Thin section: SEM photograph showing wrinkled halloysite septa (arrow), skeletal plagioclase (P) grains, and voids (black): Note K-rich feldspar (Kf) and quartz (Q) with original grain shapes which indicate slight dissolution. b) Enlarged image of the box in (a) showing the wrinkled halloysite septa (CH) coated by loose accumulations of kaolin particles (LK). Low brightness of the loose accumulation indicates the presence of many micropores. c) Untreated sample: SEM photograph of the surface of the loose accumulations showing the oriented deposition of long tubes (black arrow) and plates (white arrow).

https://doi.org/10.1346/CCMN.2000.0480205 Published online by Cambridge University Press

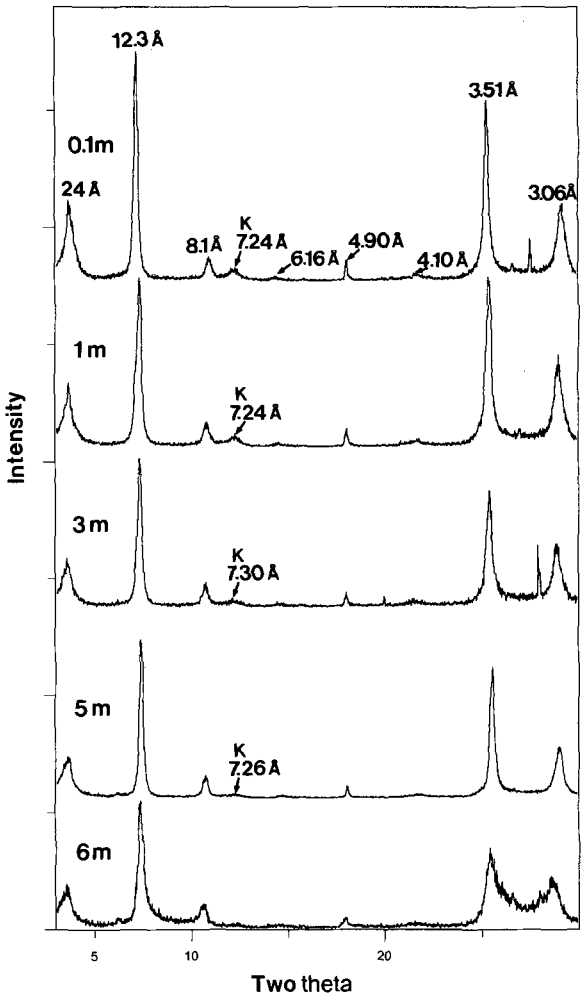

Figure 5. XRD patterns of the untreated specimens of weathered biotites. These patterns show a rational series of $d(00l)$ values of the interstratified B-V. Note the increasing peak intensities of kaolin minerals (K) upwards in the profile.

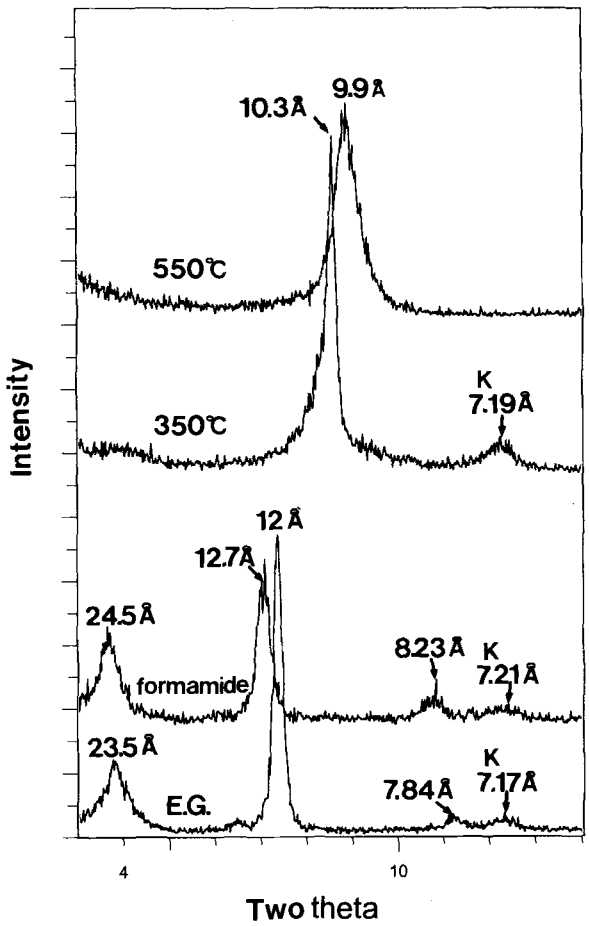

Figure 6. XRD patterns of the treated specimens of weathered biotite at a depth of 0.1 m after Mg-saturation. K: kaolinite.

0.1 m, crystals are conspicuously "fanned out" from the edges of the original grain (Figure 7b). EMA showed that B-V occurs in the grain interior but kaolin minerals had formed at the fan edge. The freshly exposed basal surface of weathered biotite at a depth of 0.1 m shows aggregates of platy kaolin minerals (Figure 7c and 7d). SEM observations confirm that the 7.24–7.30-Å phases in XRD analysis are kaolinite.

DISCUSSION

The studied granite was only partially weathered as shown by the presence of residual plagioclase in the uppermost part of the profile and nonweathered K-rich feldspar. Mineralogical and microtextural analyses of the profile showed progressive weathering of plagioclase to halloysite and biotite to kaolinite upwards in the profile. In the upper samples at depths of 0.1 and 1 m, weathered plagioclase contained some kaolinite (Figure 2). However, SEM observations suggested that the kaolinite was present in a loose aggregate with halloysite coating the preformed compact halloysite septa. Pedoturbation, raindrop splash, and runoff near the eroding surface of the soil may have dispersed kaolinite aggregates from biotite. Individual particles or small aggregates were then transported downward in suspension by rainwater and deposited on the preformed halloysite septa. The kaolinite in the weathered plagioclase of the upper samples at depths of 0.1 and 1 m originated in the comminution of kaolinitized biotite. Crystallization of halloysite and kaolinite was highly localized in weathered plagioclase and biotite, respectively.

Weathering of plagioclase to halloysite was inferred in this study and this weathering is similar to that found in the weathering profiles of anorthosite (Jeong and Kim, 1993). The different chemical compositions of plagioclase found in anorthosite (labradorite) *vs.* granite (oligoclase) suggest that the weathering pro-

https://doi.org/10.1346/CCMN.2000.0480205 Published online by Cambridge University Press

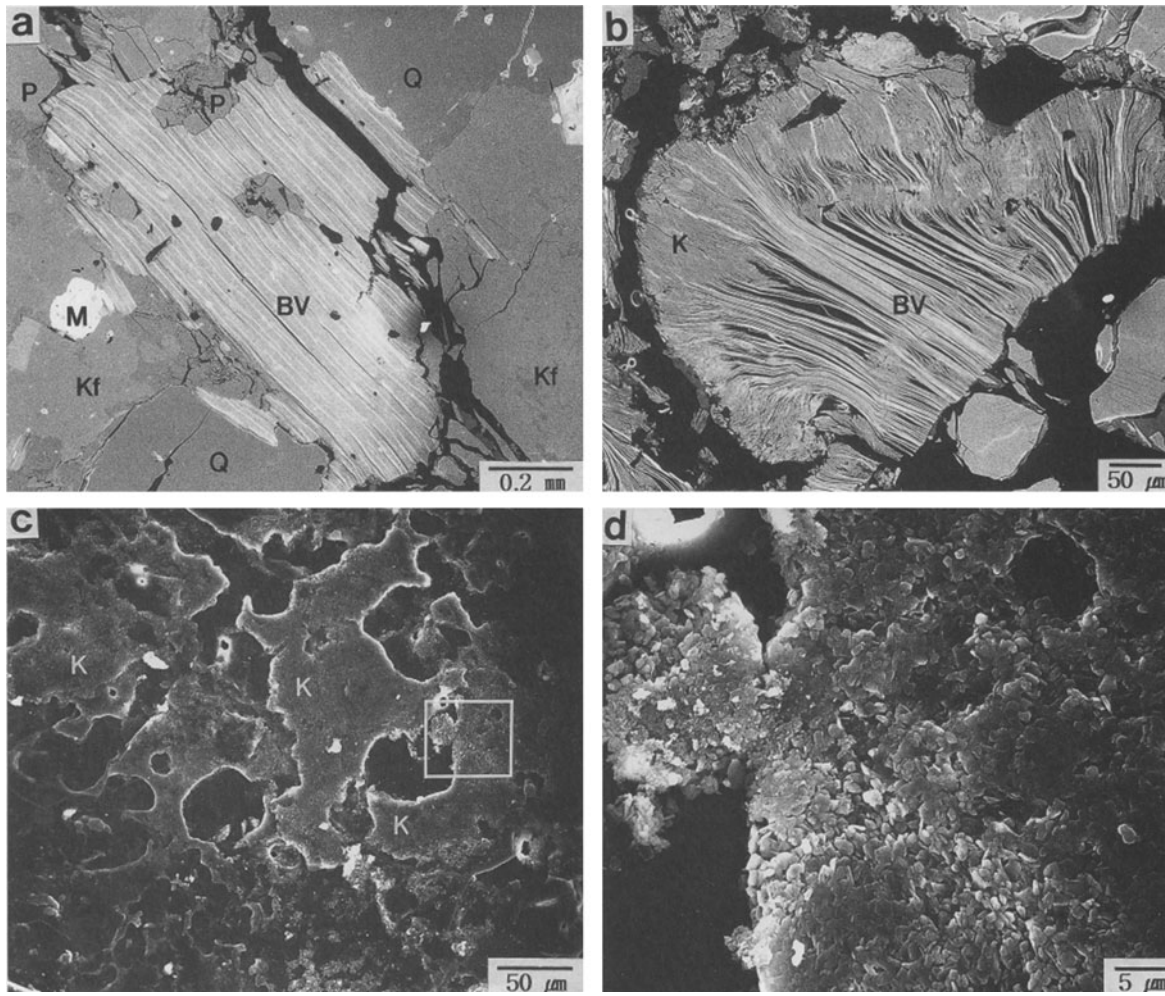

Figure 7. SEM photographs of weathered biotites. a) Regularly interstratified B-V preserving the original grain shape at a depth of 6 m. Thin section. Q: quartz, P: plagioclase, Kf: K-rich feldspar, M: magnetite. b) Weathering of B-V to kaolinite (K) with a large increase in grain volume at a depth of 0.1 m. Thin section. Black: voids. c) The freshly exposed surface of B-V in the process of kaolinitization. d) Enlarged image of the box in (c) showing the thick aggregates of kaolinite plates.

Table 3. Electron-microprobe data (wt. % oxide) of fresh and weathered biotite grains.

	Fresh rock	6 m		5 m		3 m		1 m		0.1 m	
	Analysis no.	Analysis no.		Analysis no.		Analysis no.		Analysis no.		Analysis no.	
Oxide	191	4	5	54(i)[1]	56(e)[2]	73(i)	74(e)	85(i)	86(e)	79(i)	80(e)
SiO_2	36.81	36.31	36.76	36.84	38.89	36.58	38.33	36.97	38.63	37.66	43.02
Al_2O_3	12.88	14.21	13.42	15.34	27.63	15.11	27.57	15.43	26.12	26.08	34.49
Fe_2O_3	21.15	19.35	19.72	17.21	7.75	16.78	10.90	16.85	6.56	7.68	3.09
MgO	12.96	11.40	12.48	11.47	2.77	11.26	5.73	11.38	3.69	4.19	1.09
TiO_2	5.01	4.72	5.02	4.66	0.71	5.08	0.12	5.12	1.50	1.61	0.03
MnO	0.35	0.24	0.16	0.18	0.07	0.21	0.15	0.22	0.00	0.06	0.00
CaO	0.00	0.44	0.19	0.30	0.12	0.26	0.13	0.13	0.07	0.05	0.01
K_2O	8.84	5.31	7.66	4.86	0.77	5.62	0.01	4.96	0.95	1.98	0.09
Na_2O	0.11	0.11	0.09	0.12	0.04	0.10	0.05	0.11	0.04	0.12	0.05
Total	98.11	92.07	95.51	90.98	78.74	91.01	82.99	91.16	77.56	79.43	81.87

[1] i: the interior of weathered biotite grain.
[2] e: "fan" edge.

https://doi.org/10.1346/CCMN.2000.0480205 Published online by Cambridge University Press

cess of plagioclase does not differ significantly between basic and acidic rocks.

The volume increase in the weathering of biotite is also consistent with that found in the weathering profiles of anorthosite (Jeong, 1998b), implying that such a volume change is a common phenomenon in weathering environments. The large volume increase may be explained by the thick precipitation of epitactic kaolinite on the surfaces of weathered biotite as discussed by Jeong (1998b). Because of the low Al content of biotite, large importation of Al is needed to precipitate kaolinite. Weathered plagioclase was the most important source of elements for the precipitation of kaolinite in biotite as well as for the precipitation of halloysite in plagioclase. Despite the small amount of biotite (5 wt. %) in fresh rock, this phase produced a significant mineralogical contribution to the weathering profile of granite by promoting kaolinite precipitation.

The localized crystallization of halloysite and kaolinite indicates that different physicochemical factors were operating in the microfissures of plagioclase and biotite. In thermodynamic terms, the Gibbs free energy of formation of halloysite is slightly higher than that of kaolinite (Robie and Waldbaum, 1968; Robie *et al.,* 1978; Anovitz, *et al.,* 1991), so halloysite is metastable with respect to kaolinite. In low-temperature environments, metastable phases commonly precipitate in advance of stable minerals, because of the lower activation energy of nucleation of the former (Morse and Casey, 1988; Steefel and Van Cappellen, 1990; Stumm, 1992). However, the precipitation of kaolinite may be induced by substrates that markedly lower the activation energy of nucleation. Because of its instability owing to rapid dissolution and because of its different lattice, plagioclase can not provide such a substrate. Therefore, in the microfissures of plagioclase, the nucleation of halloysite was kinetically favored over kaolinite. In contrast, the surfaces of weathered biotite grains provided suitable nucleation sites for kaolinite by dramatically decreasing the activation energy. Many previous studies reported the epitactic kaolinitization of biotite. For example, Banfield and Eggleton (1988) reported the epitactic crystallization of kaolinite packets on biotite without interstratification of kaolinite and biotite. Samotoin and Chekin (1993) observed spiral growth of kaolinite on mica substrates in weathered granite. Although Dong *et al.* (1998) and Murphy *et al.* (1998) observed the topotactic alteration of one biotite 2:1 layer to one or two 1:1 kaolinite layers in the weathering profile of quartz diorite in Puerto Rico, they also found evidence for epitactic precipitation of kaolinite in the lenticular fissures of kaolinitized biotite.

Conversion of halloysite to stable kaolinite appears to require further aging time in the studied weathering profile of granite. Surface erosion and rapid downward propagation of the weathering front might be more rapid than the conversion rate. The relative proportions of halloysite and kaolinite in the weathering profile may have been determined by the localized crystallization of halloysite in the microfissures of plagioclase and kaolinite within biotite rather than conversion. Kaolin minerals are known to be formed as the final weathering products of aluminosilicates of varying compositions or structures (Weaver, 1989), but the specific species of kaolin mineral may be strongly influenced by the primary mineralogy of the parent rock, particularly in a relatively young weathering profile. In particular, even a small amount of primary phyllosilicates induces considerable precipitation of kaolinite. For example, the vermicular kaolinites in weathered plagioclase may be at least partly derived from sericite, which is a common alteration product of plagioclase in granite before the advent of weathering (Chen *et al.,* 1997).

ACKNOWLEDGMENTS

The author thanks B. Singh, P. Schroeder, M. Velbel, and S. Guggenheim for their constructive reviews. B.Y. Lee assisted in the field and laboratory. This work was supported by project 1998-015-D00263 funded by the Korea Research Foundation.

REFERENCES

Anovitz, L.M., Perkins, D., and Essene, E.J. (1991) Metastability in near-surface rocks of minerals in the system Al_2O_3-SiO_2-H_2O. *Clays and Clay Minerals,* **39,** 225–233.

Banfield, J.F. and Eggleton, R.A. (1988) Transmission electron microscope study of biotite weathering. *Clays and Clay Minerals,* **36,** 47–60.

Banfield, J.F. and Eggleton, R.A. (1990) Analytical transmission electron microscope studies of plagioclase, muscovite, and K-feldspar weathering. *Clays and Clay Minerals,* **38,** 77–89.

Chen, P-Y., Lin, M-L., and Zheng, Z. (1997) On the origin of the name kaolin and the kaolin deposits of the Kauling and Dazhou areas, Kiangsi, China. *Applied Clay Science,* **12,** 1–25.

Churchman, G.J. and Gilkes, R.J. (1989) Recognition of intermediates in the possible transformation of halloysite to kaolinite in the weathering profiles. *Clay Minerals,* **24,** 579–590.

Churchman, G.J., Whitton, J.S., Claridge, G.G.C., and Theng, B.K.G. (1984) Intercalation method using formamide for differentiating halloysite from kaolinite. *Clays and Clay Minerals,* **32,** 241–248.

Dong, H., Peacor, D.R., and Murphy, S.F. (1998) TEM study of progressive alteration of igneous biotite to kaolinite throughout a weathered soil profile. *Geochimica et Cosmochimica Acta,* **62,** 1881–1888.

Gilkes, R.J., Suddhiprakarn, A., and Armitage, T.M. (1980) Scanning electron microscope morphology of deeply weathered granite. *Clays and Clay Minerals,* **28,** 29–34.

Jeong, G.Y. (1992) Mineralogy and genesis of kaolin in the Sancheong district, Korea. Ph.D. thesis, Seoul National University, Seoul, Korea, 325 pp.

Jeong, G.Y. (1998a) Formation of vermicular kaolinite from halloysite aggregates in the weathering of plagioclase. *Clays and Clay Minerals,* **46,** 270–279.

Jeong, G.Y. (1998b) Vermicular kaolinite epitactic on primary phyllosilicates in the weathering profiles of anorthosite. *Clays and Clay Minerals,* **46,** 509–520.

Jeong, G.Y. and Kim, S.J. (1993) Boxwork fabric of halloysite-rich kaolin formed by weathering of anorthosite in Sancheong area, Korea. *Clays and Clay Minerals,* **41,** 56–65.

Keller, W.D. (1977) Scan electron micrographs of kaolins collected from diverse environments of origin—IV. Georgia kaolin and kaolinizing source rocks. *Clays and Clay Minerals,* **25,** 311–345.

Keller, W.D., Cheng H., Johns, W.D., and Meng, C-S. (1980) Kaolin from original Kauling (Gaoling) mine locality, Kiangsi province, China. *Clays and Clay Minerals,* **28,** 97–104.

Lee, D.S. (1987) *Geology of Korea.* Kyohak-Sa, Seoul, Korea, 514 pp.

Morse, J.W. and Casey, W.H. (1988) Ostwald process and mineral paragenesis in sediments. *American Journal of Science,* **288,** 537–560.

Murphy, S.F., Brantley, S.L., Blum, A.E., White, A.F., and Dong, H. (1998) Chemical weathering in a tropical watershed, Luquillo Mountains, Puerto Rico: II. Rate and mechanism of biotite weathering. *Geochimica et Cosmochimica Acta,* **62,** 227–243.

Parham, W.E. (1969) Halloysite-rich tropical weathering products of Hong Kong. In *Proceedings of International Clay Conference, 1969, Tokyo,* L. Heller, ed., Israel University Press, Jerusalem, 403–416.

Reynolds, R.C. (1981) Interstratified clay minerals. In *Crystal Structures of Clay Minerals and Their X-ray Identification,* G.W. Brindley and G. Brown, eds., Mineralogical Society, London, 249–303.

Robertson, I.D.M. and Eggleton, R.A. (1991) Weathering of granitic muscovite to kaolinite and halloysite and of plagioclase-derived kaolinite to halloysite. *Clays and Clay Minerals,* **39,** 113–126.

Robie, R.A. and Waldbaum, D.R. (1968) *Thermodynamic Properties of Minerals and Related Substances at 298.15 °K (25°C) and One Atmosphere (1.013 bars) Pressure and at Higher Temperatures.* U.S. Geological Survey Bulletin 1259, Washington, D.C., 256 pp.

Robie, R.A., Hemingway, B.S., and Fisher, J.R. (1978) *Thermodynamic Properties of Minerals and Related Substances at 298.15 °K (25°C) and 1 Bar (10° Pascals) Pressure and at Higher Temperatures.* U.S. Geological Survey Bulletin 1452, Washington, D.C., 456 pp.

Samotoin, N.D. and Chekin, S.S. (1993) Helical growth of kaolinite crystal in layer silicates. In *Abstracts of 10th International Clay Conference, 1993, Adelaide,* South Australia, 143.

Schroeder, P.A., Kim, J.G., and Melear, N.D. (1997) Mineralogical and textural criteria for recognizing remnant Cenozoic deposits on the Piedmont: Evidence from Sparta and Greene County, Georgia, U.S.A. *Sedimentary Geology,* **108,** 195–206.

Singh, B. (1996) Why does halloysite roll?—A new model. *Clays and Clay Minerals,* **44,** 191–196.

Singh, B. and Gilkes, R.J. (1992) Weathering of a chromian muscovite to kaolinite. *Clays and Clay Minerals,* **40,** 571–579.

Singh, B. and Mackinnon, D.R. (1996) Experimental transformation of kaolinite to halloysite. *Clays and Clay Minerals,* **44,** 825–834.

Steefel, C.I. and Van Cappellen, P. (1990) A new kinetic approach to modeling water-rock interaction: The role of nucleation, precursors, and Ostwald ripening. *Geochimica et Cosmochimica Acta,* **54,** 2657–2677.

Stumm, W. (1992) *Chemistry of the Solid-Water Interface.* John Wiley & Sons, New York, 428 pp.

Weaver, C.E. (1989) *Clays, Muds, and Shales.* Elsevier, Amsterdam, 819 pp.

E-mail of corresponding author: geoyoung@chollian.net

(Received 12 April 1999; accepted 16 October 1999; Ms. 332; A.E. Michael Velbel)